Transfer ionization and its sensitivity to the ground-state wave function

M. S. Schöffler[1], O. Chuluunbaatar[2,3], Yu. V. Popov[4], S. Houamer[5], J. Titze[1], T. Jahnke[1], L.Ph.H. Schmidt[1], O. Jagutzki[1], A. G. Galstyan[6] and A. A. Gusev[2]

[1]Institut für Kernphysik, University Frankfurt, Frankfurt, Germany
[2]Joint Institute for Nuclear Research, Dubna, Russia
[3]School of Mathematics and Computer Science, National University of Mongolia, UlaanBaatar, Mongolia
[4]Skobeltsyn Institute of Nuclear Physics, Moscow State University, Moscow, Russia
[5]Département de physique, Faculté de Sciences, Université Ferhat Abbas, Sétif, Algeria
[6]Physics Faculty, Moscow State University, Moscow, Russia

galstyan@physics.msu.ru

Introduction

A theory which is capable to predict all the experimental observed data for transfer ionization (TI) is a particular worthy goal as there are many indications in the literature that transfer ionization is an extremely interesting channel, whose rich features cannot be accessed by photon, ion or electron impact double ionization or in strong laser pulses. In this poster we consider the simplest TI reaction $\mathbf{H^+ + He \rightarrow H + He^{2+} + e^-}$.
Emission of the second electron in this reaction can take place via shake-off (SO) due to sudden removal of its correlation partner in the bound state (Fig. 1 $\boldsymbol{A_1 + A_3}$) or as a result of direct collision with the projectile (so called binary encounter, BE, FBA version in the Fig. 1 $\boldsymbol{A_2}$). Higher Born terms contribute to BE mechanism as well. After the first collision with a fast bare projectile a fast electron is ejected from the bound state. Subsequent (elastic) collisions with the nucleus in the intermediate state do not change its velocity too much. The intermediate $\boldsymbol{e-e}$ interaction in contrast needs a more careful treatment.
We present the experimental distribution of the momentum of the escaped electron in the scattering plane and the corresponding calculations in the PWFBA on the level of fully differential cross sections. By comparing these calculations to our high-resolution experimental data, we separate ionization due to shake-off ($\boldsymbol{A_1 + A_3}$) or binary collision ($\boldsymbol{A_2}$) (see Fig. 1) leading to distinct islands in momentum space. One of the results is that these data are extremely sensitive to the initial-state correlation.

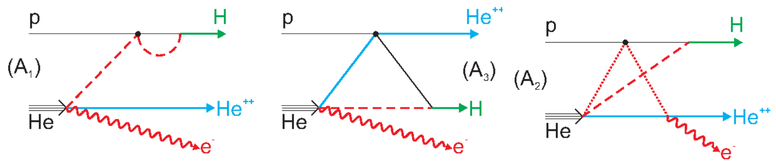

Figure 1: $\boldsymbol{A_1}$ and $\boldsymbol{A_3}$ describes the terms due to shake-off (SO) mechanism. Term $\boldsymbol{A_2}$ describes the BE amplitude.

Experiment

We have used the COLTRIMS technique [6, 7, 8] to determine the momentum vectors of all final-state products. The experiment was performed at the Van de Graaff accelerator of the Institut für Kernphysik at the University of Frankfurt. The projectile beam (H^+) was collimated to a size of about 0.5 x 0.5 mm^2 at the target. 15 cm upstream of the target, a set of electrostatic deflector plates cleaned the primary beam from charge state impurities. The proton beam intersects with a supersonic helium gas jet (density of $\mathbf{5 \times 10^{11}}$ atoms/cm^2 and a diameter of 1 mm). About 15 cm downstream a second set of electrostatic deflector plates separate the final charge state, thus only the neutral projectiles (H) hit a position and time sensitive multichannel plate (MCP) detector [9, 10] yielding the projectile deflection angle and the time zero of the collision. The recoil ions were accelerated by a weak electrostatic field of 4.8 V/cm in the interaction region and detected on a 80 mm MCP-detector with delay-line anode. To optimize the resolution, a three dimensional time and space focussing geometry [11, 12] was used for the spectrometer. A momentum resolution of 0.1 a. u. was achieved in all three directions. The electrons were guided by a magnetic field of 15-25 Gauss and accelerated by the same electric field in a time focussing geometry [13] onto a multi channel plate detector of 120 mm active diameter. A three-particle coincidence (H-He^{2+}-e) was applied to record the data event-by-event. From the positions of impact on the detectors and the time-of-flight we can derive the initial momentum vectors of the He^{++} and the electron. Energy conservation was used for off-line background suppression. Furthermore the high resolution data allowed to distinguish data where the neutral projectile H is found in an excited state from those, where the hydrogen is in its ground-state [14]. Only these latter ones are presented in this poster.

Theory

Let us denote the projectile proton momentum by $\vec{p}_p$, the hydrogen momentum by $\vec{p}_H$, and the recoil-ion momentum by $\vec{K}$. We also define the transferred momentum as $\vec{q} = \vec{p}_H - \vec{p}_p$. We can deduce its approximate value using the momentum and energy conservation

$$\vec{q} + \vec{K} + \vec{k} = \mathbf{0}, \tag{1}$$

$$\frac{p_p^2}{2m} + E_0^{He} = \frac{p_H^2}{2(m+1)} + \frac{K^2}{2M} + E^H + E^{ion}. \tag{2}$$

Here $\vec{k}$ is the ejected electron momentum, the proton mass $m = \mathbf{1836.15}$, the helium ion mass $M \approx 4m$, $E_0^{He} = -\mathbf{2.903724377034}$, and $E^{ion} = k^2/2$.
Now we choose very small scattering angles for the outgoing hydrogen ($0 \leq \theta_p \lesssim 0.5$ mrad). It leads to a practically zero ion velocity K/M in the laboratory frame during the process, and we can consider the ion like immovable. The proton velocity $\vec{v}_p = \vec{p}/m$ varies about a few a.u. for its energy of several hundredths keV. This fact allows one to neglect $K^2/2M$ and $q^2/2m$ after insertion of $\vec{p}_H = \vec{q} + \vec{p}_p$ into eq. (2). As a result we obtain

Theory

$$\vec{v}_p\vec{q} = \frac{1}{2}v_p^2 + Q; \quad Q = E_0^{He} - E^H - E^{ion}, \tag{3}$$

and choose the vector $\vec{v}_p$ as z-axis; there follows $q_z = v_p/2 + Q/v_p$The x-component of the vector is $q_x = (\vec{p}_H)_x \approx mv_p\theta_p$.
In the presented experiments, the scattering plane $\{z, x, y = 0\}$ formed by the momentum vectors $\vec{p}_p$ (z-axis) and $\vec{p}_H$ is fixed in space, and we put its polar angle $\phi = 0$. The corresponding triple differential cross section (TDCS) takes the form

$$\frac{d^3\sigma}{dk_x dk_z d\phi} = \frac{m^2}{(2\pi)^5} \int_{\theta_i}^{\theta_{i+1}} \theta_p d\theta_p \int_{-\infty}^{\infty} dk_y |A_1 + A_2 + A_3|^2. \tag{4}$$

Here (θ_i, θ_{i+1}) is the scattering angle domain and (k_x, k_y, k_z) the electron momentum components. We calculate the TDCS depending on (k_z, k_x) electron momentum distribution in the scattering plane. We omit in short the mathematical and kinematical details of description of the symmetrized matrix elements $\boldsymbol{A_1}$, $\boldsymbol{A_2}$ and $\boldsymbol{A_3}$, which are given in [16].
In theoretical calculations we use two trial ground-state helium wave functions. One is the loosely correlated $\mathbf{1s^2}$ Roothaan-Hartree-Fock (RHF) wave function [15] (no angular correlation) with a rather poor ground-state energy of -2.861680 a. u. Another one is the highly correlated wave function given in [17] with a ground-state energy of -2.903721 a. u. being very close to the experimental value of -2.903724377034 a. u..

Results and discussion

In the Fig. 2 we present experimental electron momentum distributions and theoretical results in the scattering plane defined by the incoming projectile direction and the scattered projectile (the x-component of the vector $\vec{p}_H$ is positive here). Only events for a small projectile scattering angle $\theta_p \leq$0.25 mrad are selected. The experimental data in Fig. 2a show that at these small scattering angles, the electron is predominantly emitted in backward direction.

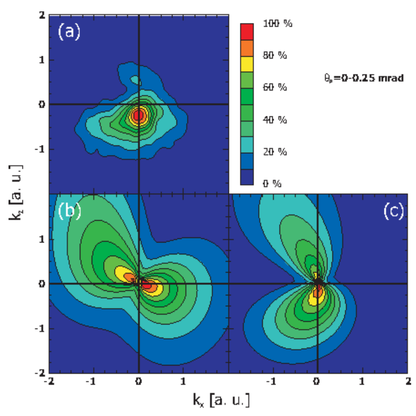

Figure 2: Experimental and theoretical data for 630 keV H+/He collisions for $\theta_p \leq \mathbf{0.25}$ mrad. (a) are the experimental data and the red dashed line represents the binary encounter ridge. (b) calculations using a helium $\mathbf{1s^2}$ trial wave function, while (c) uses a highly correlated helium wave function with angular momentum, all including terms $\boldsymbol{A_1 + A_2 + A_3}$.

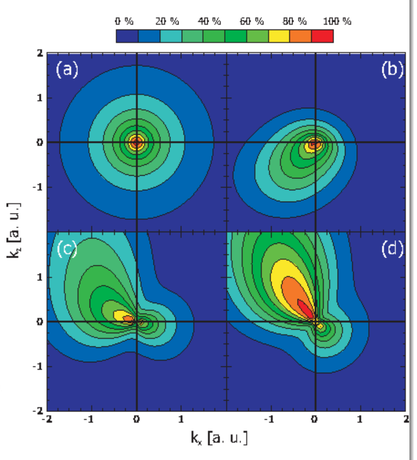

Figure 3: Calculations for $\theta_p \leq \mathbf{0.25}$ and helium $\mathbf{1s^2}$ trial wave function separated in SO (a) and TS2 (c) contributions. Similar calculations for highly correlated helium wave function are presented in panels (b) and (d).

The results using a $\mathbf{1s^2}$ trial helium wave function are shown in Fig. 2b. For small θ_p the momentum distribution is very similar to the binary- and recoil-peak structures (forward and backward) well known from electron impact ionization experiments [18]. For comparison, the separation of the individual contributions/processes is shown in Fig. 3. The expected electron momentum distribution for the shake-off-process ($\boldsymbol{A_1 + A_3}$-term) in the case of loosely correlated helium wave function is shown in the top row (Fig. 3a), while in Fig. 3c (lower row) only the sequential TS2 mechanism ($\boldsymbol{A_2}$-term) is taken into account. The shake-off exhibits a perfectly isotropic behavior, as expected for a $\mathbf{1s^2}$-state with zero angular momentum. This term has however a visible influence on the coherent sum of the different contributions $\boldsymbol{A_1}$ + $\boldsymbol{A_2}$ + $\boldsymbol{A_3}$ (Fig. 2c) despite of a small overall dominance of slight dominance of the $\boldsymbol{A_2}$ (TS2) term (the maximum in Fig. 3a is $\mathbf{5.75 \times 10^{-7}}$, while in Fig. 3c it is $\mathbf{9.00 \times 10^{-7}}$; the total maximum in Fig. 2b is $\mathbf{7.00 \times 10^{-7}}$). It changes the binary/recoil peak ratio, while conserving the general features of forward and backward contributions leaving the overall distributions to be similar.
Comparing the experimental and theoretical results presented in Fig. 2a and Fig. 2b, we find notable differences.
The agreement improves considerably for a well-correlated helium wave function with radial and angular $\boldsymbol{e-e}$ correlations. In Fig. 2c the results of our calculations are shown again for small θ_p values. And they are split into the different contributions in Fig. 3 (b,d). The maximum in Fig. 3b is $\mathbf{1.3 \times 10^{-6}}$, while in Fig. 3d it is $\mathbf{6.25 \times 10^{-7}}$; the total maximum in Fig. 2c is $\mathbf{1.6 \times 10^{-6}}$. It can clearly be seen that the shake-off terms in Fig 3b show an asymmetric emission pattern (about 3 times larger compared to Fig. 3a), peaking in backward direction.

Results and discussion

A binary/recoil peak-like structure is clearly visible again for the $\boldsymbol{A_2}$-term using a correlated wave function (Fig. 3d). The coherent sum (Fig. 2c) also exhibits two clearly distinct non-equal peaks pointing forward and backward along the z-axis. This structure is considerably rotated clockwise compared to the one shown in Fig. 2b. Both calculations (Fig. 2c) and the experiment (Fig. 2a) demonstrate predominantly the backward electron emission. However, detailed investigations of SO and TS2 contributions show that the term $\boldsymbol{A_2}$ is still big and leads to an overestimate in the forward scattering domain.
It is necessary to say a few words about contributions of second and higher order Born terms. After collision with the fast projectile proton the electron gets a rather high velocity and moves predominantly in the forward direction. It keeps this direction after elastic scattering on the atomic nucleus or another electron. We expect that the SO electrons are well described within FBA, whereas BE (TS2) electrons are more effected by higher (second) Born terms. As a consequence we can expect that the FBA term overestimates the contribution of forward scattered electrons (FBA and SBA matrix elements have different signs in total).

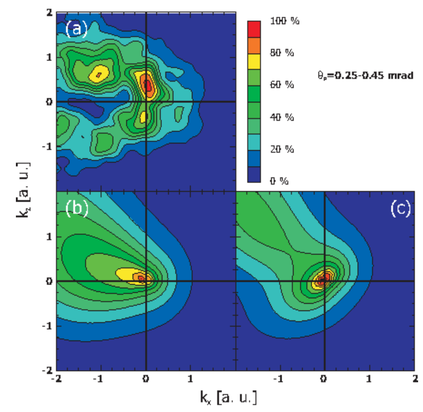

Figure 4: The same like in Fig. 2, but for $\mathbf{0.25} \leq \theta_p \leq \mathbf{0.45}$ mrad.

We now consider plots corresponding to larger scattering angles $0.25 \leq \theta_p \leq$0.45 mrad (Fig. 4). The experiment (Fig. 4a) shows a richer of spots predominantly in forward direction and opposite to the x-component of $\vec{p}_H$. Now the FBA results (Fig. 4b for loosely correlated and Fig. 4c for highly correlated helium wave functions) are less structured. The correlated wave function displays some "pinch" structure at $\{k_x \sim -\mathbf{1}, k_z \sim \mathbf{0.4}\}$, which we can be seen in Fig. 4a; but the main peak is well centered around $\{k_x = \mathbf{0}, k_z = \mathbf{0}\}$, while the experimental peak is notably shifted towards larger k_z. The predominant emission to the fourth quadrant is a result of rather hard binary collision which are selected in the plot by the projectile scattering angle.

Conclusion

In conclusion, we present highly differential theory (PWFBA) and experimental data from a kinematical complete experiment on transfer ionization in proton-helium collision at 630 keV/u. The observed splitting into forward and backward emission originates from two different contributions, the $\boldsymbol{A_2}$-term (TS2, electron knock-off) and the $\boldsymbol{A_1 + A_3}$-term (shake-off). Comparison of a loosely and a strongly correlated wave function for the initial state confirms the high sensitivity of the experiment to the subtle features of the initial state wave function. FBA more or less explains the experiment at very small scattering angles and small electron momenta, but the SBA calculations are needed to improve results in forward scattering domain $k_z > \mathbf{0}$. At bigger angles the SBA calculations are strongly needed.

References

1 A. Godunov, C. T. Whelan, and H. R. J. Walters, J. Phys. B: At. Mol. Opt. Phys., **37,** L201, (2004).
2 M. Schöffler *et. al, J. Phys. B: At. Mol. Opt. Phys.*, ***38,*** *L123, (2005).*
3 J. H. McGuire *et. al, Phys. Rev. A,* ***38,*** *3333, (1988).*
4 J. H. McGuire and L. Weaver, Phys. Rev. A, **16,** 41, (1977).
5 A. Knapp *et. al, Phys. Rev. Lett.,* ***89,*** *033004, (2002).*
6 J. Ullrich *et al., J. Phys. B: At. Mol. Opt. Phys.,* ***30,*** *2917, (1997).*
7 R. Dörner *et al., Physics Reports,* ***330,*** *95, (2000).*
8 J. Ullrich *et al., Rep. Prog. Phys.,* ***66,*** *1463, (2003).*
9 O. Jagutzki *et al., Nucl. Instr. and Meth. in Phys. Res. A,* ***477,*** *256, (2002).*
10 O. Jagutzki *et al., Nucl. Instr. and Meth. in Phys. Res. A,* ***477,*** *244, (2002).*
11 M. S. Schöffler *et al., New Journal of Physics,* ***13,*** *095013, (2011).*
12 V. Mergel *et al., Phys. Rev. Lett.,* ***74,*** *2200, (1995).*
13 W. C. Wiley, I. H. McLaren, Rev. Sci. Instr., **26,** 1150, (1955).
14 H.-K. Kim *et al., Phys. Rev. A,* ***85,*** *022707, (2012).*
15 Enrico Clementi and Carla Roetti. Atomic Data and Nuclear Data Tables **14**, 177 (1974).
16 S. Houamer, Yu. V. Popov, and C. Dal Cappello, Phys. Rev. A **81**, 032703 (2010).
17 O. Chuluunbaatar *et al., Phys. Rev. A* ***74****, 014703 (2006).*
18 H. Ehrhardt *et al.,* ***1,*** *3-32, (1986).*